



# Evaluation of commercially available polylactic acid (PLA) filaments for 3D printing applications

Bruna Driussi Mistro Matos<sup>1</sup> · Valmir Rocha<sup>3</sup> · Eraldo Jannone da Silva<sup>3</sup> · Franco Henrique Moro<sup>3</sup> · Alex Camilli Bottene<sup>3</sup> · Clovis Augusto Ribeiro<sup>5</sup> · Diogenes dos Santos Dias<sup>5</sup> · Selma Gutierrez Antonio<sup>5</sup> · André Capaldo do Amaral<sup>1,3</sup> · Sandra Andrea Cruz<sup>4</sup> · Helida Gomes de Oliveira Barud<sup>2</sup> · Hernane da Silva Barud<sup>1</sup>

Received: 15 June 2018 / Accepted: 4 December 2018 / Published online: 17 December 2018  
© Akadémiai Kiadó, Budapest, Hungary 2018

## Abstract

Poly(lactic acid) (PLA) is a biodegradable and bioresorbable biopolymer that has successfully been applied in biomedical and related fields. It is in the form of filaments, presenting different colors, with the purpose to be used in the three-dimensional printing (3D) technique. Thus, this work aimed to characterize five commercially available PLA filaments which were differentiated by color, as follows: blue (1), gray (2), transparent (3), orange (4) and natural (5) comparing to a pellet pattern. Thermal characterization was performed throughout simultaneous thermogravimetry (TG), derivative thermogravimetry (DTG), differential thermal analysis (DTA) and differential scanning calorimetry (DSC). Significant differences in the enthalpies and temperatures of crystallization and melting indicated differences in crystallinity of the filaments corroborated by the XRD analysis. While analyzing using TG/DTG–DTA, significant differences in thermal stability were observed. The absorption spectroscopy in the infrared was also done to determine the chemical composition of the samples. Additionally, it was also observed the structure, size and roughness of the filaments using confocal microscopy building three-dimensional images. The oscillatory rheometer was employed to determine the complex viscosity ( $\eta^*$ ), the storage modulus ( $G'$ ) and the loss modulus ( $G''$ ) as a function of frequency ( $\omega$ ). After conducting the characterizations, it was possible to compare the five types of PLA filaments and identify the best one to feature a functionalization in the future, which possibly enable them in tissue engineering applications. Results indicated that the blue filament fulfilled the best results regarding print quality, higher-temperature degradation and thermal stability, with the molar mass and viscosity superior to the other filaments.

**Keywords** PLA filaments · Confocal microscopy · FTIR spectra · Thermal stability · XRD · Rheological analysis

---

✉ Clovis Augusto Ribeiro  
clovis.ribeiro@unesp.br  
Hernane da Silva Barud  
hernane.barud@gmail.com

<sup>1</sup> Biopolymers and Biomaterials Laboratory - UNIARA, Carlos Gomes Street 1217, Araraquara 14801-340, Brazil

<sup>2</sup> Biosmart Nanotechnology, Araraquara, Brazil

<sup>3</sup> São Paulo University - USP, Trabalhadores São-carlense Avenue, São Carlos 13566-590, Brazil

<sup>4</sup> Department of Chemistry, Center for Exact and Technological Sciences, Federal University of São Carlos - UFSCar, Jardim Guanabara, São Carlos, SP 13565-905, Brazil

<sup>5</sup> São Paulo State University IQ/UNESP, Professor Francisco Degni Street 55, Araraquara 14800-060, Brazil

## Introduction

With the increasing popularity and scientific interests, the additive manufacturing process or 3D printing is undoubtedly one of the technologies to follow in the twenty-first century. The 3D printing technique was originated around the 1980s, and the first patent was approved in 1986. Regarding 2014, the US National Aeronautics launched the first 3D printer whose parts were built in zero gravity. This extraordinary advance enabled 3D printing to become increasingly popular [1]. After that, 3D printing has been characterized to be a remarkable method by which objects can be built by merging or deposition of materials. This process is carried out layer by layer until the final shape of the object is obtained [2]. In recent years, 3D printing technologies have consistently contributed to advances in regenerative medicine approaches, mainly about bone tissues. Therefore, it is possible to produce tailored devices suited to the need and extent of the injury to be repaired. Within regenerative medicine strategies, these devices can be found in metal for use as orthopedic implants in bone defects (osteosynthesis devices) or biological carriers in the form of scaffolds [1, 3]. One of the most affordable three-dimensional printing methods for biomedical applications is the fused deposition modeling (FDM) process, being one of the techniques that characterize the rapid prototyping technology presenting the high potential for use in bone regenerative medicine. This technique is based on the use of thermoplastic filaments consisting in polymers or polymer/ceramic composites, which are extruded and deposited layer by layer resulting in specific three-dimensional structures [1]. Concerning bone regenerative medicine, for example, it is necessary to use specific software based on computer-aided design (CAD) which recreate geometric models from images obtained of the body segments previously established by computed tomography or magnetic resonance imaging. An additional step regarding processing images is determined by its transverse sections allowing the slicing, and each section will be used as a template for scheduled printing of each layer. Thus, it is worth stressing out some advantages of 3D printing technique throughout additive manufacturing, such as low-cost process at rates much lower than traditional ones, reproducibility and easy processability with better quality and less waste, new shapes and structures presenting higher durability and structural integrity and also the possibility to obtain new combinations of materials [4]. Then, 3D technology has been successfully applied in the medical field with the creation of uniquely shaped devices for each type of patient [5]. Because of continuous innovation, these devices can be created by various types of biomaterials that act in the regeneration of

damaged tissues, which are biocompatible offering distinguished applications, including ceramics, metals and glass [6, 7]. PLA is classified as a biopolymer that can be obtained from renewable sources (corn, beet, cassava, among others) being biodegradable and useful for biomedical applications, configuring one of the most promising polymers for this area. Moreover, PLA is widely used in bone fixation sutures, tissue engineering and drug delivery systems [8] because the process of PLA degradation occurs by simple hydrolysis of ester bonds being metabolized by the human body without requiring the action of enzymes which prevents inflammatory reactions [9]. Comparing to other biopolymers, PLA is more hydrophobic because it owns a methyl group which is more soluble in organic solvents [10]. There are two types of commercially available PLA. One is PLLA (L-lactic acid), and the other is PDLA (D, L-lactic), differing from PLA regarding properties such as crystallinity and melting temperature [11]. In contrast, constraints inherent to nature, quality and processability of polymers represent one of its disadvantages [4]. The uniformity, continuity and diameter of the filaments play an essential role in the FDM process [12], and these characteristics may influence the strength and durability of its. Therefore, the main objective of this work is to accomplish with the morphological, thermal and structural characterization of commercially available PLA filaments to verify which one will possibly enable additive manufacturing and functionalization. After this first step, all information acquired may point out PLA filaments as excellent materials to construct scaffolds/ implants in tissue engineering applications.

## Materials and methods

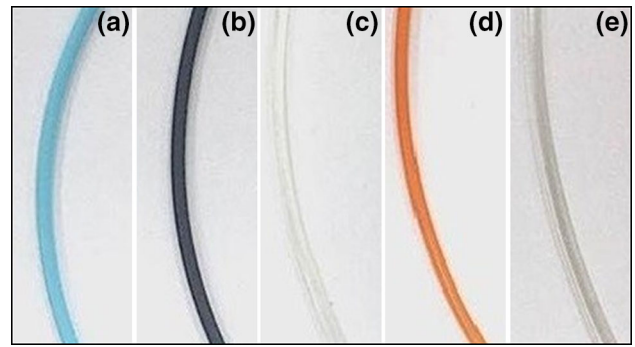
Commercially available filaments of different colors and companies were used. Confocal microscopy was performed using the Olympus LEXT OLS4100 digital laser scanning microscope non-contact 3D. This microscopy is so sensitive that it easily enables observations and measurements of the surface at 10-nanometer resolutions with fast image acquisition and high-resolution microscope images over a wider area. This analysis performed for visualization of samples, increasing the contrast of images, constructing three-dimensional images, observing the structure, size and roughness of the filaments. After viewing the images, we compare each type of PLA (polylactic acid) filament, differentiated by color, where five colors were analyzed filaments: blue, gray, transparent, orange and natural. These strands are approximately 1.75 mm in diameter and found significant differences. Confocal microscopy was performed in NUMA Department (advanced manufacturing core), located in the School of Engineering of São Carlos,

University of São Paulo—Campus São Carlos. Samples were renamed PLA-1 (blue), PLA-2 (gray), PLA-3 (transparent), PLA-4 (orange) and PLA-5 (natural), and throughout the text, figures and tables in the types of PLA will be presented in numbers, as mentioned. The average thickness and standard deviation of the filaments of each sample were measured with the digital caliper—ZAAS Precision, provided by QUIMMERA laboratory located in UNIARA—Unit 2—Araraquara. TG/DTG-DTA curves were obtained by a TA Instruments SDT 2960 Simultaneous to evaluate the thermal decomposition of PLA filament samples using nitrogen atmosphere ( $100 \text{ mL min}^{-1}$ ) at a heating rate of  $20 \text{ }^\circ\text{C min}^{-1}$  and temperature range of 30 to  $600 \text{ }^\circ\text{C}$  to evaluate the thermal stability. DSC curves used to evaluate the thermal events such as glass transition, crystallization and melting for samples of PLA filaments in blue, gray, orange, colorless and natural pattern. We used a nitrogen atmosphere ( $100 \text{ mL min}^{-1}$ ), a heating rate of  $10 \text{ }^\circ\text{C min}^{-1}$  and sample mass of approximately 6 mg. DSC curves were obtained in the DSC1 Mettler, open aluminum crucible and static air atmosphere. Analyses performed at the Chemistry Institute of the So Paulo State University—Campus Araraquara. The vibrational spectroscopy in the infrared region was performed using FTIR Spectrometer Vertex 70 Bruker with accessory ATR (attenuated total reflectance). This analysis was also performed at the Institute of Chemistry of the São Paulo State University—Campus Araraquara. The crystallinity of the samples was measured using an X-ray diffractometer D8 Advance, Bruker. This analysis was carried out at a  $2\theta$  range between  $4^\circ$  and  $80^\circ$  with a step size of  $0.02^\circ$  in a continuous mode of  $1^\circ \text{ min}^{-1}$ , a  $2.5^\circ$  divergence Soller slit and position-sensitive detector—LynxEye. All refinements and fits were performed with TOPAS Academic 5.0 [13]. An oscillatory rheometer (Anton Paar MCR 302) was employed to determinate the complex viscosity ( $\eta^*$ ), the store modulus ( $G'$ ) and the loss modulus ( $G''$ ) as a function of frequency ( $\omega$ ). It was used 25-mm-diameter plates and a gap of the 1.0 mm at a temperature of  $190 \text{ }^\circ\text{C}$ . The range of frequency was  $0.1\text{--}500 \text{ rad s}^{-1}$  at 2% strain, which was proved to be in the linear viscoelastic range.

## Results and discussion

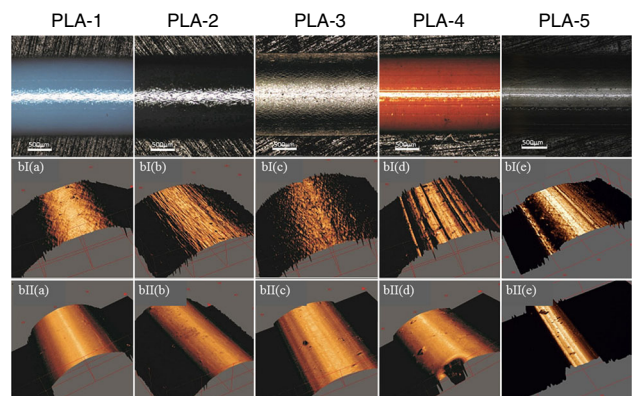
### Morphological characterization

Figure 1 shows a digital photograph of commercially available PLA samples studied in this work. All filaments are macroscopically homogeneous and have an average thickness of between 1.72 and 1.76 mm, which is consistent with the report provided by the manufacturers.



**Fig. 1** PLA filaments **a** (PLA-1) blue; **b** (PLA-2) gray; **c** (PLA-3) transparent; **d** (PLA-4) orange; **e** (PLA-5) natural. (Color figure online)

Figure 2 shows confocal microscopy data of all PLA filament before and after extrusion. As seen in bI images (a), bI (b), bI (c), bI (d) and bI (e) before extrusion there are grooves and grain traits in all PLA filaments. Thus, the filaments before extrusion show a heterogeneous appearance, because of the stages of production of PLA filament material conducted to this aspect, with grooves and grains. It was noted that after the filament is extruded, a more smooth and homogeneous aspect is acquired as shown in bII images (a), bII (b), bII (c), bII (d) and bII (e). There are differences in print quality after heating to  $240 \text{ }^\circ\text{C}$  by the printer extrusion nozzle with a nominal diameter of 0.6 mm. When the material is not in the form of a filament, it is subjected to various stages of production, such as drying, changes in time and instrumentation. Due to improper drying, climate change and instrumentation material end up getting a non-uniform appearance. If the correct temperature for the production of filaments is used, we have the moisture removal, and a better control the extrusion, and consequently the material will be processed uniformly and



**Fig. 2** Digital photography of PLA filaments. (bI) Confocal microscopy of different PLA filaments before (bII) confocal microscopy of different PLA filaments after extrusion. The white bar at the filaments before extrusion is equivalent to 500 micrometers

with better thickness. Table 1 shows the thickness data (mean), standard deviation and surface roughness of each of the PLA filaments before and after extrusion, and the extruder nozzle of the 3D printer.

## Structural characterization

### FTIR spectra

FTIR spectra of the samples of PLA and PLA filament pellets are shown in Fig. 3. The most intense band observed is observed in the spectrum shown in Fig. 3; all PLA samples are located in  $1750\text{ cm}^{-1}$ , which is associated with the stretching C=O (hydroxyl) of the ester group, and this group belongs to the polylactic acid chain. The most striking peaks in  $1750\text{ cm}^{-1}$  and  $2747\text{ cm}^{-1}$  correspond to aldehydic CH stretching vibration band and C=O stretching vibration during the degradation of PLA, the most significant peaks with the peaks  $2930$  and  $3010\text{ cm}^{-1}$  stretching CH vibration and  $1380$  and  $1445\text{ cm}^{-1}$   $\text{CH}_3\text{-CH}$  bending vibration, showing that the aldehyde is formed [14]. The  $\text{CH}_3$  appears in  $1460\text{ cm}^{-1}$ ; this is the asymmetrical angular deformation. The band  $1180\text{ cm}^{-1}$  and  $1085\text{ cm}^{-1}$  is observed to be associated with possible asymmetrical axial deformation modes of Bester (O–C–C). The region  $1300\text{--}900\text{ cm}^{-1}$  contains several coupled strips. The major bands between  $1300$  and  $1500\text{ cm}^{-1}$  are symmetrical relating to the angular deformation of the C–H bond of the methylene ( $\text{CH}_2$ ) and methyl ( $\text{CH}_3$ ) [15]. The peaks  $1180$ ,  $1359$  and  $1270\text{ cm}^{-1}$  represent the elongation (C–C), and the peak of  $1454\text{ cm}^{-1}$  is the flexure (CH) [16]. These peaks are observed in all samples of commercially available PLA filaments. Thus, FTIR confirms that the PLA filaments have a similar chemical profile to standard pellet.

### X-ray diffraction—XRD

Figure 4 shows the amorphous halo and the characteristic peak of the PLA. Both crystallinity and the crystallite size were calculated using routines implemented in TOPAS Academic 5.0. The crystallite size is calculated to the nearest double-Voigt approach. The change in crystallinity

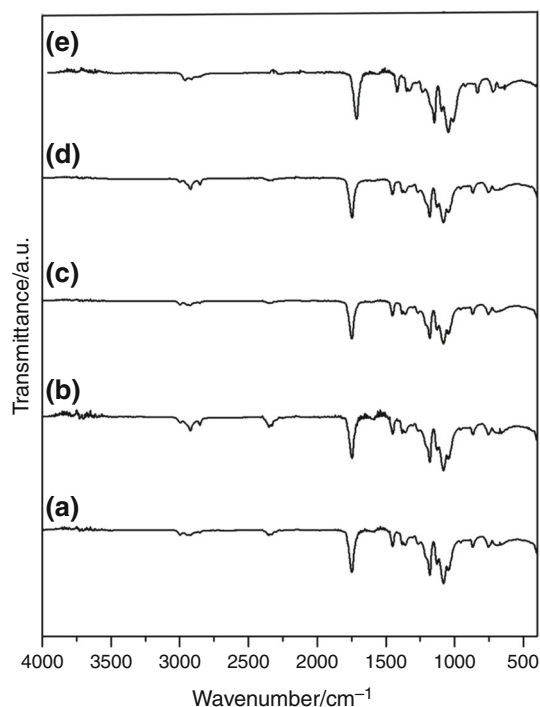


**Fig. 3** Infrared spectrum for PLA filaments (PLA-1) blue; (PLA-2) gray; (PLA-3) transparent; (PLA-4) orange and (PLA-5) natural

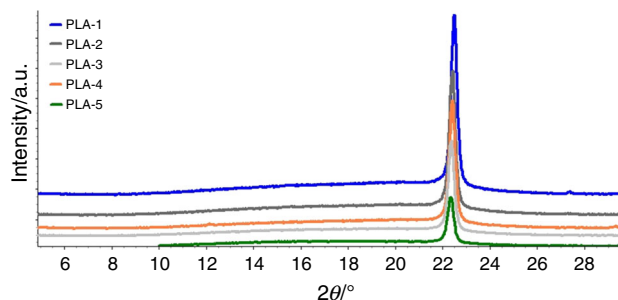


**Fig. 4** XRD curves for PLA filaments (PLA-1) blue; (PLA-2) gray; (PLA-3) transparent; (PLA-4) orange and (PLA-5) natural. (Color figure online)

and crystallite size exhibits the same order of magnitude with little difference in the natural sample, however, with an increase in crystallinity (Table 2).

**Table 1** Data filaments (thickness/standard deviation and roughness)

Filaments	Thickness (average)/mm	Roughness before extrusion/ $\mu\text{m}$	Roughness after extrusion/ $\mu\text{m}$
PLA-1	$1.72 \pm 0.02$	$0.27 \pm 0.3$	$0.08 \pm 0.02$
PLA-2	$1.76 \pm 0.04$	$0.54 \pm 0.1$	$0.06 \pm 0.04$
PLA-3	$1.76 \pm 0.04$	$1.72 \pm 1.1$	$0.07 \pm 0.03$
PLA-4	$1.73 \pm 0.01$	$0.44 \pm 0.2$	$0.10 \pm 0.01$
PLA-5	$1.74 \pm 0.02$	$0.10 \pm 0.5$	$0.11 \pm 0.02$



**Table 2** Crystallinity and the crystallite size calculated from XRD

Filaments	Crystallinity/%	Crystallite size/nm
PLA-1	39.78	31.65
PLA-2	36.61	28.26
PLA-3	33.76	28.04
PLA-4	38.46	42.68
PLA-5	25.35	27.05

**Table 3** Data obtained from TG/DTG curves for PLA filaments

Filaments	$T_{\text{onset}}$	$T_i$	$T_f$	Residue/% 600 °C
PLA-1	326.0	270.8	395.6	0.4275
PLA-2	333.6	274.2	372.3	1.1290
PLA-3	338.8	278.7	376.9	0.5943
PLA-4	327.9	258.3	372.2	0.4013
PLA-5	288.9	248.7	341.1	0.8575

## Thermal characterization

### TG/DTG and DTA curves

TG and DTG curves (Fig. 5a, b) allowed verifying the differences in thermal stability for PLA filaments containing different pigments. TG/DTG curves for PLA from samples 1 to 5 show a single step of thermal decomposition in the range of 240–390 °C. It can be observed that the presence of colored pigment increased the stability of PLA filament on the natural PLA (Table 3).

DTA curves (Fig. 6) show a change in baseline between 100 and 200 °C without mass loss in TG curves, characteristic for glass transition,  $T_g$ , of PLA, however, with variations depending on the pigment composition of the polymer. This aspect has better evaluated in the DSC curves (Fig. 7). Between 200 and 300 °C can observe the endothermic peak related to the thermal decomposition of the polymers in an atmosphere of nitrogen.

### DSC curves

DSC curves (Fig. 7) show the heating from 25 to 80 °C when it can be seen glass transition of the polymer along

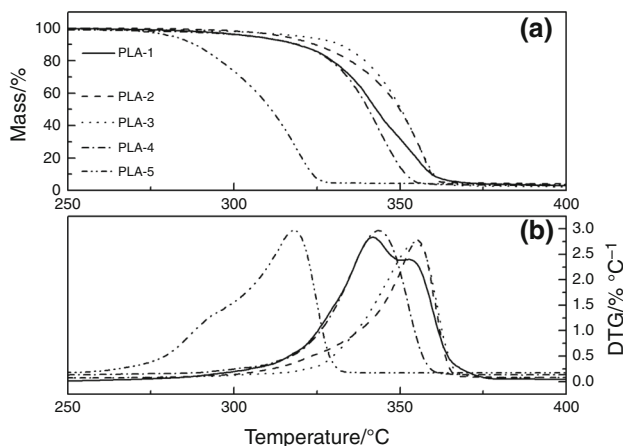


**Fig. 5** TG(A)/DTG(B) curves for PLA filaments (PLA-1) blue; (PLA-2) gray; (PLA-3) transparent; (PLA-4) orange; (PLA-5) natural, in nitrogen atmosphere (100 mL min<sup>-1</sup>) at heating rate of 20 °C min<sup>-1</sup>

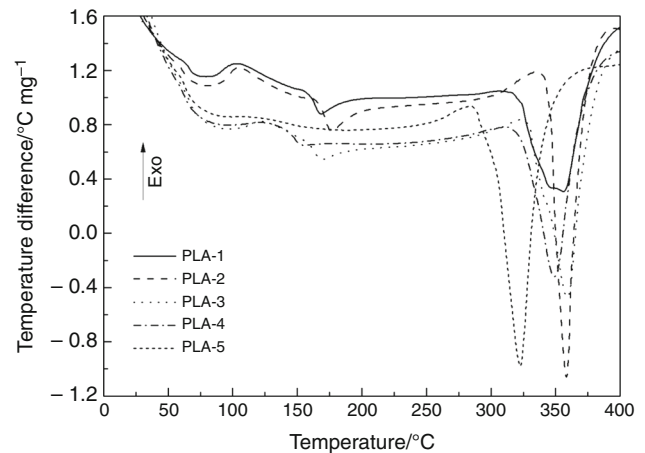


**Fig. 6** DTA curves for PLA filaments (PLA-1) blue; (PLA-2) gray; (PLA-3) transparent; (PLA-4) orange; (PLA-5) natural, in nitrogen atmosphere (100 mL min<sup>-1</sup>) at heating rate of 20 °C min<sup>-1</sup>

with relaxation peak. It is no longer observed exothermic cold crystallization peak,  $T_{\text{onset}}$  among 86–105 °C depending on pigmented filaments and is probably dependent on the prior heat treatment in the extruder. The endothermic melting peak can be observed from 140 to 180 °C also depending on the pigment present and the prior heat treatment in the extruder by the PLAs. Table 4 presents the glass transition temperature and the enthalpy of crystallization ( $\Delta H_c$  J g<sup>-1</sup>) calculated from DSC curves. The standard sample did not present crystallization peak, indicating that filament already presented with maximum crystallinity, before heat treatment by the DSC curve.

For polymers that present cold crystallization during heating is necessary the temperature-dependent crystallinity method approach [17, 18]. Thus, from values of enthalpy of fusion at the melting point and enthalpy of crystallization at the crystallization peak given in Table 4, one could calculate the mass fraction extent of crystallinity measured at different temperatures and without correction for changes in specific heat [19, 20],  $X_c$  given by:

$$X_c = \frac{\Delta H_f(T_m) - \Delta H_c(T_c)}{\Delta H_f^0(T_m^0)} \quad (1)$$

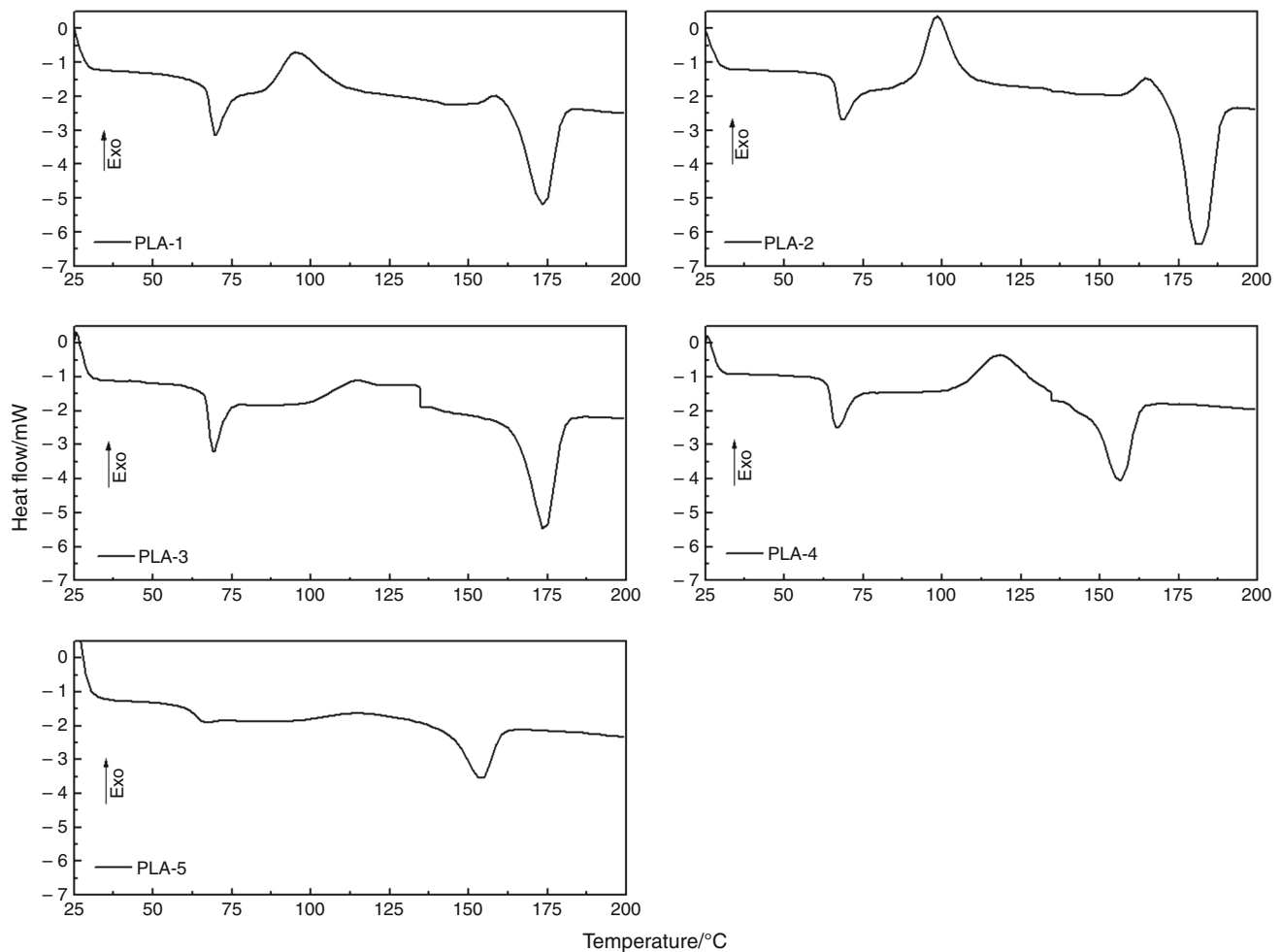


**Fig. 7** DSC curves for PLA filaments **a** PLA-1 (blue); **b** PLA-2 (gray); **c** PLA-3 (transparent); **d** PLA-4 (orange); **e** PLA-5 (natural), in static air at heating rate of  $10\text{ }^{\circ}\text{C min}^{-1}$

**Table 4** Data obtained from DSC curves for PLA filaments

Filaments	$T_g$		$\Delta H_c/\text{J g}^{-1}$	$T_c$ onset/ $^{\circ}\text{C}$	$\Delta H_f/\text{J g}^{-1}$	$T_m$ onset/ $^{\circ}\text{C}$	$T_m$ peak/ $^{\circ}\text{C}$	Crystallinity	
	onset	MID						$X_c/\%$ Eq. (2)	$X_c/\%$ Eq. (1)
PLA-1	58.06	61.38	21.25	86.08	31.89	164.33	173.59	34.13	11.39
PLA-2	59.30	62.46	23.53	91.94	45.35	174.29	181.03	48.21	23.19
PLA-3	58.36	61.61	20.66	101.19	31.00	165.64	173.91	33.14	11.05
PLA-4	56.02	59.29	18.65	105.05	24.98	147.37	156.32	26.75	6.77
PLA-5	60.10	62.75			16.67	144.03	154.01	17.77	17.77

where  $\Delta H_f^0(T_m^0)$  is the enthalpy of fusion to utterly crystalline polymer measured at the equilibrium melting point,  $T_m^0$  [21].

Disregarding the cold crystallization, we will have the maximum crystallization of the filaments considering only the melting temperature, given by:

$$X_c = \frac{\Delta H_f(T_m)}{\Delta H_f^0(T_m^0)} \quad (2)$$

The considered enthalpy of fusion to utterly crystalline PLA measured at the equilibrium melting point,  $\Delta H_f^0$ , has a value of  $93\text{ J g}^{-1}$  [22]. The calculated values for crystallinity degree discounted the residue in TG curves

(Table 3) and then converted to a percentage, which are given in Table 4. Crystallinity obtained through data from the DSC curves, although not obtained in equilibrium conditions, presents discrepancies with those obtained by XRD (Table 2). The PLA filament manufacturer does not report the amount of dyes and other additives. These dyes and additives may be organic and thus are being thermally decomposed together with the PLA polymer and are not being considered in the calculation of crystallinity through the DSC curves, justifying the discrepancy concerning the XRD.

These differences in crystallinity, together with the difference in temperature and enthalpy of crystallization and melting, indicate that there may be differences in size and polydispersity of the PLA chain, as can be seen in the rheological analysis. Consequently, differences in thermal stability by TG and DTA analysis can be observed (Figs. 5 and 6) (Table 3). It also may indicate, as a consequence, different conditions during printing on a 3D printer

### Rheological analysis

Figure 8 presents the complex viscosity as a function of frequency for the PLA samples.

It is possible to observe that all the samples present a Newtonian behavior, at low frequencies, followed by a pseudoplastic behavior, at higher frequencies. The PLA-1 sample has the largest molar mass with complex viscosity approximately 140,000 Pa.s at 0.1 rad s<sup>-1</sup>. On the other hand, the PLA-2 sample has the lowest molar mass with 80,000 Pa.s in the same frequency range. This behavior is more accentuated for the samples of lower molar mass (PLA-2, PLA-4 and PLA-3). This increase in the viscosity could be associated with esterification and transesterification reactions [23] that are favored for lower initial molar mass. The higher temperature combined with the inert

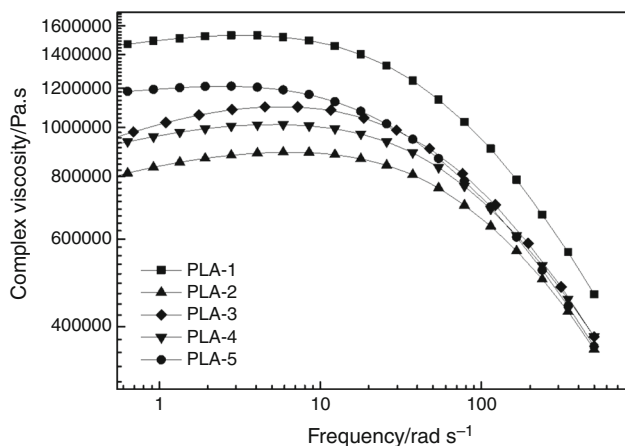


Fig. 8 Complex viscosity of the samples as a function of frequency

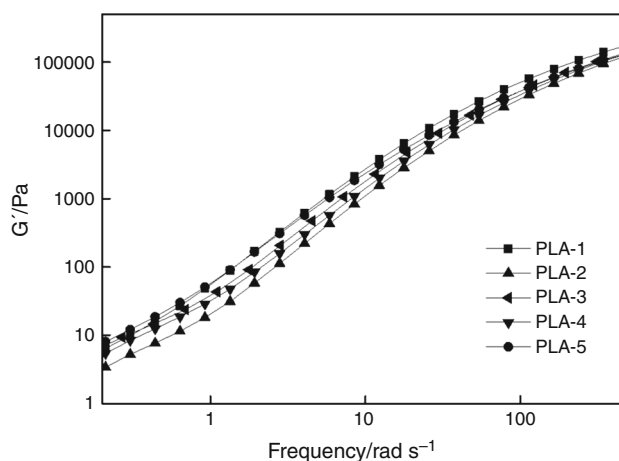


Fig. 9 Storage modulus as a function of frequency for PLA samples

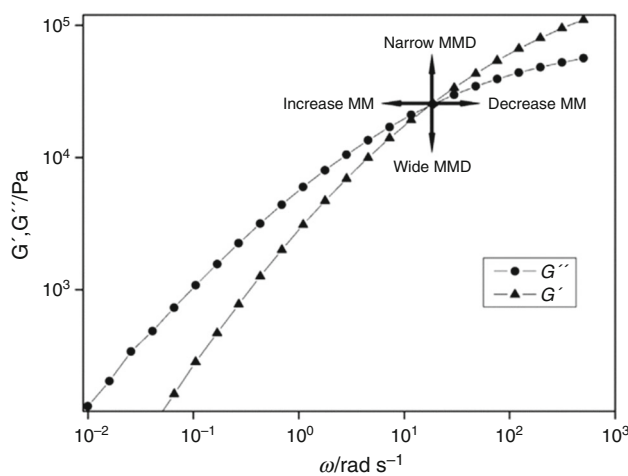


Fig. 10 Curves of  $G'(\omega)$  and  $G''(\omega)$  for a hypothetical polymer indicating variations of the molar mass and molar mass distribution according to crossover point ( $G' = G''$ ) [24]

atmosphere prevented the thermo-oxidative process and favored reactions, resulting in a slight increase in molar mass.

Figure 9 presents the storage modulus ( $G'$ ) as a function of frequency. This property is dependent on the molar mass, that is, the level of entanglements. So, the higher the molar mass, the higher the numbers of entanglements and the  $G'$  values.

Changes in the molar mass, as well as molar mass distribution, could be determined by the crossover point at which  $G' = G''$  (Fig. 10). The results obtained by the PLA samples are presented in Table 5.

As can be observed, the samples follow the same trend of molar mass, corroborating the results of viscosity as a function of frequency: PLA-1 > PLA-5 > PLA-3 > PLA-2 > PLA-4. On the other hand, PLA-1 and PLA-4 samples

**Table 5** Crossover point (where  $G' = G''$ ) and frequency ( $\text{rad s}^{-1}$ ) for the PLA samples

Samples	$\omega/\text{rad}$	$G' = G''/\text{Pa}$
PLA-1	318.86	$13.37 \times 10^4$
PLA-2	491.25	$12.67 \times 10^4$
PLA-3	391.91	$11.86 \times 10^4$
PLA-4	510.94	$13.35 \times 10^4$
PLA-5	382.40	$11.46 \times 10^4$

have a narrow molar mass distribution and PLA-3 and PLA-5 the wider distributions.

## Conclusions

In this work, commercially available PLA filaments were physicochemically characterized regarding morphological, structural and thermal properties. By confocal measurements, it is possible to see that after the extrusion process all PLA filaments acquired a smoother and homogeneous aspect. TG/DTG/DTA curves revealed different thermal stability as a function of the PLA filaments' color, and DSC curves and XRD diffractograms were able to determine the crystallinity aspects of the commercial PLA filaments. By oscillatory rheometer, it is possible to observe that all the samples present a Newtonian behavior, at low frequencies, followed by a pseudoplastic behavior, at higher frequencies. The PLA-1 sample presents the largest molar mass and a narrow molar mass distribution than the other one. Differences in crystallinity, crystallite size, enthalpy and temperature of crystallization and melting, chain size and polydispersity of PLA had a consequence on their thermal stability. However, these differences in filament behavior may indicate different conditions to be observed when printing to 3D printers. Even so, commercial PLA filaments could be an alternative to produce medical devices for tissue engineering applications shortly.

**Acknowledgements** The authors acknowledge the FAPESP for financial support.

## References

- Bandyopadhyay A, Bose S, Das S. 3D printing of biomaterials. *MRS Bull.* 2015;40:108–15.
- Ventola CL. Medical applications for 3D printing: current and projected uses. *Pharm Ther.* 2014;39:704–11.
- Chia HN, Wu BN. Recent advances in 3D printing of biomaterials. *J Biol Eng.* 2015;9:1–14.
- Hoque ME, Chuan YL, Pashby I. Extrusion based rapid prototyping technique: an advanced platform for tissue engineering scaffold fabrication. *Biopolymers.* 2012;97:83–93.
- Takagaki LK. Tecnologia de impress 3D. In: Alessandro Marco Rosini, editor. *Revista Inovao Tecnolgica.* So Paulo; 2012. p. 28–40.
- Rengier F, Mehndiratta A, von Tengg-Kobligk H, Zechmann CM, Unterhinninghofen R, Kauczor HU, Gieser FL. 3D printing based on imaging data: review of medical applications. *Int J Comput Assist Radiol Surg.* 2010;5:335–41.
- Gross BC, Erkal JL, Lockwood SY, Chen C, Spence DM. Evaluation of 3D printing and its potential impact on biotechnology and the chemical sciences. *Anal Chem.* 2014;86:3240–53.
- Lopes SM, Jardini AL, Filho RM. Poly (lactic acid) production for tissue engineering applications. *Proc Eng.* 2012;42:1402–13.
- Lasprilla AJ, Martinez GA, Lunelli BH, Jardini AL, Filho MR. Poly-lactic acid synthesis for application in biomedical devices—a review. *Biotechnol Adv.* 2012;30:321–8.
- Ndazi BS, Karlsson S. Characterization of hydrolytic degradation of polylactic acid/rice hulls composites in water at different temperatures. *Express Polym Lett.* 2011;5:119–31.
- Carrasco F, Pages P, Prez-Gmes J, Santana OO, MasPOCH ML. Processing of poly(lactic acid): characterization of chemical structure, thermal stability and mechanical properties. *Polym Degrad Stab.* 2010;95:116–25.
- Murphy CA, Collins MN. Microcrystalline cellulose reinforced polylactic acid biocomposite filaments for 3D printing. *Polym Compos.* 2018;39:1311–20.
- Coelho A. TopasAcademic Version 5. In: Coelho Software. Brisbane, Australia; 2007. <http://www.topas-academic.net>. Accessed 15 Jan 2017.
- Zou H, Yi C, Wang L, Liu H, Weilin X. Thermal degradation of poly(lactic acid) measured by thermogravimetry coupled to Fourier transform infrared spectroscopy. *J Therm Anal Calorim.* 2009;97:929–35.
- Drumond WS, Wang SH, Moth CG. Sntese e caracterizao do copo-mero poli(cido ltico-b-glicol etilnico). *Polmeros Cincia e Tecnologia.* 2004;14:74–9.
- Chapple S, Anandjiwala R, Sinha RS. Mechanical, thermal, and fire properties of polylactide/starch blend/clay composites. *J Therm Anal Calorim.* 2013;113:703–12.
- Gray AP. Polymer crystallinity determinations by DSC. *Thermochim Acta.* 1970;1:563–79.
- Mathot VBF. *Calorimetry and thermal analysis of polymers.* New York: Hanser Publications; 1994.
- Kong Y, Hay JN. The measurement of the crystallinity of polymers by DSC. *Polymer.* 2002;43:3873–8.
- Kong Y, Hay JN. The enthalpy of fusion and degree of crystallinity of polymers as measured by DSC. *Eur Polym J.* 2003;39:1721–7.
- Allegra G, Corradini P, Elias HG, Geil PH, Keith HD. Definitions of terms relating to crystalline polymers (Recommendations 1988). *Pure Appl Chem.* 1989;61:769–85.
- Fischer EW, Sterzel HJ, Wegner G. Investigation of the structure of solution grown crystals of lactide copolymers by means of chemical reaction. *Kolloid-Zu Z-Polymer.* 1973;251:980–90.
- Peng B, Hou H, Song F, Wu L. Synthesis of high molecular weight poly(l-lactic acid) via melt/solid state polycondensation. II. Effect of precrystallization on solid state polycondensation. *Ind Eng Chem Res.* 2012;51:5190–6.
- Garcia PS, Scuaraccio CH, Cruz SA. Effect of residual contaminants and of different types of extrusion processes on the rheological properties of the post-consumer polypropylene. *Polym Test.* 2013;32:1237–43.